Undulation instability in block-copolymer lamellae subjected to a perpendicular electric field

Mark W. Matsen

Received 3rd August 2006, Accepted 18th September 2006
First published as an Advance Article on the web 17th October 2006
DOI: 10.1039/b611064a

We examine the stability of lamellar stacks in the presence of an electric field, E_0, applied normal to the lamellae. Calculations are performed with self-consistent field theory (SCFT) supplemented by an exact treatment of the electrostatic energy for linear dielectric materials. The calculations identify a critical electric field, E_0^*, beyond which the lamellar stack becomes unstable with respect to undulations. This E_0^* rapidly decreases towards zero as the number of lamellae in the stack diverges. Our quantitative predictions for E_0^* are consistent with previous experimental measurements by Xu and co-workers.

1. Introduction

AB diblock copolymers are long-chain molecules of N segments, where the first fN are of type A and the remaining $(1 - f)N$ are of type B. In their liquid (or melt) state, the natural tendency for the unlike A and B blocks to segregate (typically measured by the Flory–Huggins χ parameter) results in the formation of various periodically-ordered morphologies.[1] Researchers are now exploiting this self-assembly as a means of fabricating nanoscale structures,[2] either directly from the block-copolymer material,[3] as scaffolds for arranging other molecules/nanoparticles[4,5] or as templates for nanolithography.[6] Possible applications/devices include high-density information storage,[6] waveguides,[7] nanoporous membranes[3,4] and nanowires.[5,8] Although the self-assembly process is exceptionally efficient, it does not always produce the desired pattern; the common examples being that lamellar and cylindrical domains tend to orient parallel to the substrate, as opposed to perpendicular where they exhibit a more useful lateral structure. Researchers[9] have coated the substrates to negate the surface interactions that cause this, but the resulting morphologies are generally populated by numerous defects. One strategy for overcoming this problem is to orient the domains using strong electric fields that couple to the contrast between the dielectric constants, κ_A and κ_B, of the A and B components.[10,11]

Fig. 1 illustrates the morphology of parallel lamellae that naturally forms when the diblocks are symmetric ($f \approx 0.5$) and the plates possess an affinity for one of the components. With the application of a sufficient electric field, $E_0 \geqslant E_0^*$, the lamellae become unstable with respect to undulations, and ultimately reorient in the perpendicular direction. Onuki and Fukuda[12] have previously predicted the critical field, E_0^*, where the undulatory mode goes unstable, and Xu *et al.*[13,14] have subsequently examined the effect of an electric field, $E_0 \approx 40$ V μm^{-1}, on symmetric polystyrene-polymethylmethacrylate (PS-PMMA) diblock copolymer films with thicknesses equal to v = 4, 10, 23, and 100 lamellar layers. However, the relevance of the predicted E_0^* to the experiment is compromised by the fact that Xu and co-workers applied their electric field before the films had a chance to form well-ordered lamellae. Nevertheless, quantitative comparison with the theory would have been complicated by the fact that Onuki and Fukuda used a phenomenological model that assumes a sinusoidal composition profile of amplitude, $2A$, and assigns the lamellar layers a compressibility, B, and a bending modulus, K. Thus, a direct comparison would require further calculations[15] to relate the phenomenological parameters (*e.g.*, A, B and K) to the actual molecular parameters (*e.g.*, χ, N and f).

We have recently developed a full microscopic approach based on self-consistent field theory (SCFT) supplemented by an exact treatment of the electric-field effects. Not only does the calculation predict the critical field, E_0^*, in terms of the microscopic parameters, it does so with fewer approximations

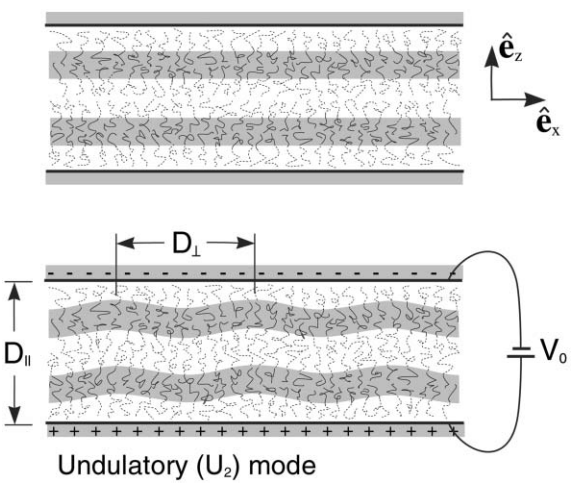

Fig. 1 The top panel shows a 2-layer stack of parallel lamellae. The bottom panel illustrates an undulation mode of wavelength, $D_\perp$, that becomes unstable when the electric field, $E_0 \equiv V_0/D_\parallel$, exceeds a critical value, E_0^*.

Department of Physics, University of Reading, Whiteknights Campus, Reading, United Kingdom RG6 6AF. E-mail: m.w.matsen@reading.ac.uk

than the Onuki–Fukuda approach. In our previous study,[16] however, we restricted our attention to monolayer films ($v = 1$), which are much thinner than those studied in experiment. Therefore, we revisit the problem, this time examining thicker multilayer films.

2. Theory

Our original letter[16] only provides a brief outline of the theoretical method, and so we now present it in more detail. We begin by first defining a model for the system in Fig. 1, specifically a melt of n monodisperse AB diblock copolymers confined between two parallel conducting plates of area, $\mathscr{A}$, located at $z = 0$ and $D_{\|}$. As with most microscopic approaches, we use standard Gaussian chains[17] where the polymers are divided into large course-grained segments defined according to a common volume of ρ_0^{-1}, such that total volume of the film is $\mathscr{V} \equiv \mathscr{A}D_{\|} = nN/\rho_0$. Note that the assumption of a fixed segment volume implies that the melt is incompressible. The segments are assumed to contain a sufficient number of chemical monomers such that the entropic free energy associated with their internal degrees of freedom imparts them with an effective elasticity, the modulus of which is specified by a_A and a_B, the statistical lengths of A- and B-type segments, respectively. Thus the diblock copolymers are treated as thin elastic threads with two chemically distinct ends that interact by an unfavourable contact force.

Despite the simplicity of this model, the statistical mechanics cannot be performed exactly given the large number of mutually interacting molecules. To proceed, the mean-field approximation is implemented, whereby each polymer interacts with the average (*i.e.*, mean) positions of the other molecules rather than their actual positions. By doing this, the interactions on the A and B segments can be represented by static fields, $w_A(\mathbf{r})$ and $w_B(\mathbf{r})$, respectively. This is often supplemented with additional approximations based on the fields being either very weak or very strong,[17] but here we use self-consistent field theory (SCFT) in which no further approximations are imposed.

SCFT is made feasible by an effective method for solving the statistical mechanics of a single Gaussian chain subjected to static fields.[18] The principle challenge is to calculate the probability distribution, $\rho(\mathbf{r},s)$, for a given segment, specified by a parameter s that increases uniformly along the polymer backbone from $s = 0$ at the A-end to $s = 1$ at the B-end. This probability is evaluated by considering the Boltzmann weight of all configurations, where the s-th segment is pinned at $\mathbf{r}$. Because the energies of the $[0,s)$ and $(s,1]$ portions of the chain are independent, the distribution,

$$\rho(\mathbf{r},s) = \frac{\mathscr{V}}{\mathscr{Q}} q(\mathbf{r},s)\bar{q}(\mathbf{r},s) \tag{1}$$

is proportional to the product of $q(\mathbf{r},s)$, the partial partition function for the $[0,s)$ chain fragment, and $\bar{q}(\mathbf{r},s)$, the analogous function for the $(s,1]$ fragment. The normalization factor,

$$\mathscr{Q} \equiv \int q(\mathbf{r},s)\bar{q}(\mathbf{r},s)d\mathbf{r} \tag{2}$$

is in fact the single-chain partition function. The first partial partition function is obtained by starting from the initial condition, $q(\mathbf{r},0) = 1$, and applying the differential equation,

$$\frac{\partial}{\partial s} q(\mathbf{r},s) = \left\{ \frac{a_\gamma^2 N}{6} \nabla^2 - w_\gamma(\mathbf{r}) \right\} q(\mathbf{r},s) \tag{3}$$

where $\gamma = A$ for $s < f$ and $\gamma = B$ for $s > f$.[18] The second function is solved using $\bar{q}(\mathbf{r},1) = 1$ and the same diffusion eqn (3) but with $\partial/\partial s$ replaced by $-\partial/\partial s$. Because Gaussian chains are completely flexible, the two confining plates can be treated with reflecting boundary conditions.[18] Once $\rho(\mathbf{r},s)$ is known, the A- and B-segment concentrations are given by

$$\phi_A(\mathbf{r}) = \int_0^f \rho(\mathbf{r},s)ds \tag{4}$$

$$\phi_B(\mathbf{r}) = \int_f^1 \rho(\mathbf{r},s)ds \tag{5}$$

respectively.

In the spirit of mean-field theory, the free energy, F, of the film is

$$\begin{aligned} \frac{F}{nk_BT} = &-\ln \mathscr{Q} + \frac{1}{\mathscr{V}} \int \{\chi N \phi_A(\mathbf{r})\phi_B(\mathbf{r}) \\ &- w_A(\mathbf{r})\phi_A(\mathbf{r}) - w_B(\mathbf{r})\phi_B(\mathbf{r}) \\ &+ H(\mathbf{r})N(\phi_A(\mathbf{r}) - \phi_B(\mathbf{r}))\} d\mathbf{r} - \mathscr{E} \end{aligned} \tag{6}$$

The logarithmic term represents the free energy of the molecules subjected to the mean fields, while the integral adds to that the energy from the A–B segment interactions and removes the fictitious energy from the mean fields. The integral also includes an interaction energy due to the surface potential,

$$H(\mathbf{r}) \equiv 2\{\Lambda_1 \delta(z) + \Lambda_2 \delta(z - D_{\|})\} aN^{1/2} \tag{7}$$

where Λ_1 and Λ_2 specify the affinity for A-type segments at the $z = 0$ and $D_{\|}$ plates, respectively. We do not apply a surface affinity in this current study, but nevertheless we included it in the theory for the sake of completeness.

The last term in eqn (6) represents the electrostatic energy stored in the film,

$$\mathscr{E} nk_BT = \frac{1}{2} V_0 Q$$

where $\pm Q$ is the total charge on the conducting plates. It may seem strange that this energy is subtracted from F rather than added, but the argument for doing so is simple. When the morphology varies, there will be a flow of charge, $\mathrm{d}Q$, to the plates in order to maintain a constant V_0, and this will cause the electrostatic energy to change by $V_0\mathrm{d}Q/2$. However, we must not forget that the energy of the power supply changes by $-V_0\mathrm{d}Q$. Thus the net energy change is $-V_0\mathrm{d}Q/2$, which is exactly what we get if we omit the power supply and simply reverse the sign of $\mathscr{E} nk_BT$.[10]

Since it is difficult to evaluate Q, the electrostatic energy is calculated instead by the well-known expression,[10]

$$\mathscr{E} nk_BT = \frac{\varepsilon_0}{2} \int \kappa(\mathbf{r}) |\mathbf{E}(\mathbf{r})|^2 d\mathbf{r} \tag{8}$$

where the relative electric permittivity of the film is assumed to obey the simple-mixing form,

$$\kappa(\mathbf{r}) \equiv \kappa_A \phi_A(\mathbf{r}) + \kappa_B \phi_B(\mathbf{r}) \tag{9}$$

which interpolates between the values, κ_A and κ_B, for pure A- and B-type polymers, respectively. (Our calculations will not be particularly sensitive to the precise form of $\kappa(\mathbf{r})$ because they focus on well segregated melts.) Following this approach, the calculation of $\mathscr{E}$ only requires the electric field, $\mathbf{E}(\mathbf{r})$, between the plates, which obeys the Maxwell equation, $\nabla\cdot[\kappa(\mathbf{r})\mathbf{E}(\mathbf{r})] = 0$. Since the electric force is conservative, the field can be expressed as

$$\mathbf{E}(\mathbf{r}) = -E_0 \nabla v(\mathbf{r}) \tag{10}$$

which transforms the Maxwell equation into

$$\nabla\kappa(\mathbf{r})\cdot\nabla v(\mathbf{r}) + \kappa(\mathbf{r})\nabla^2 v(\mathbf{r}) = 0 \tag{11}$$

Since we wish to investigate instabilities in the morphology created by the application of an electric field, we examine the Landau–Ginzburg functional, $F[\Phi]$, for the free energy of a composition profile specified by

$$\phi_A(\mathbf{r}) - \phi_B(\mathbf{r}) = \Phi(\mathbf{r}) \tag{12}$$

$$\phi_A(\mathbf{r}) + \phi_B(\mathbf{r}) = 1 \tag{13}$$

These two conditions are satisfied by suitably adjusting their conjugate fields,

$$w(\mathbf{r}) \equiv \frac{w_A(\mathbf{r}) - w_B(\mathbf{r})}{2} \tag{14}$$

$$u(\mathbf{r}) \equiv \frac{w_A(\mathbf{r}) + w_B(\mathbf{r})}{2} \tag{15}$$

respectively. Substituting these conditions into eqn (6) provides the free-energy functional,

$$\begin{aligned}\frac{F[\Phi]}{nk_BT} = &-\ln \mathscr{Q} + \frac{1}{\mathscr{V}}\int\left\{\frac{\chi N}{4}\left(1-\Phi^2(\mathbf{r})\right)\right.\\ &-w(\mathbf{r})\Phi(\mathbf{r}) - u(\mathbf{r})\\ &\left.+H(\mathbf{r})N\Phi(\mathbf{r})\right\}d\mathbf{r} - \mathscr{E}\end{aligned} \tag{16}$$

Note that the equilibrium free energy of the film, F, is given by the global minimum of $F[\Phi]$.

To simplify the theory, we now expand the spatially-varying quantities in Fourier series,

$$f(\mathbf{r}) = \sum_{\mathbf{k}} f_{\mathbf{k}} \exp(i\mathbf{k}\cdot\mathbf{r}) \tag{17}$$

summed over the wavevectors,

$$\mathbf{k} \equiv \frac{2\pi n_x}{D_\perp}\hat{\mathbf{e}}_x + \frac{\pi n_z}{D_\parallel}\hat{\mathbf{e}}_z \tag{18}$$

where n_x and n_z are integers. For the time being, we present the theory assuming only that functions such as $f(\mathbf{r})$ are real, which implies $f_{-\mathbf{k}} = f_{\mathbf{k}}^*$. In the end, we will enforce the reflecting boundary conditions at $z = 0$ and $D_\parallel$ by requiring real Fourier coefficients with $f_{\mathbf{k}} = f_{\bar{\mathbf{k}}}$, where

$$\bar{\mathbf{k}} \equiv \frac{2\pi n_x}{D_\perp}\hat{\mathbf{e}}_x - \frac{\pi n_z}{D_\parallel}\hat{\mathbf{e}}_z \tag{19}$$

Since the electric potential satisfies different boundary conditions, we expand it as

$$v(\mathbf{r}) = -z - i\sum_{\mathbf{k}\neq 0} v_{\mathbf{k}} \exp(i\mathbf{k}\cdot\mathbf{r}) \tag{20}$$

For now, we only assume $v_{-\mathbf{k}} = -v_{\mathbf{k}}^*$, but ultimately we will require real coefficients with $v_{\mathbf{k}} = v_{\bar{\mathbf{k}}}$ so that $v = 0$ at $z = 0$ and $v = -D_\parallel$ at $z = D_\parallel$.

In terms of Fourier coefficients, the diffusion eqn (3) for $q(\mathbf{r},s)$ becomes

$$\frac{d}{ds}q_{\mathbf{k}}(s) = \sum_{\mathbf{g}} \left[\mathbf{S}_\gamma\right]_{\mathbf{k},\mathbf{g}} q_{\mathbf{g}}(s) \tag{21}$$

where the components of the two Hermitian matrices, $\mathbf{S}_A$ for $s < f$ and $\mathbf{S}_B$ for $s > f$, are

$$\left[\mathbf{S}_\gamma\right]_{\mathbf{k},\mathbf{g}} = -\frac{k^2 a_\gamma^2 N}{6}\delta_{\mathbf{k},\mathbf{g}} - w_{\gamma;\mathbf{k}-\mathbf{g}} \tag{22}$$

This simple set of first-order linear differential eqn (21) is solved by constructing the transfer matrices, $\mathbf{T}_\gamma(s) \equiv \exp(\mathbf{S}_\gamma s)$, for $\gamma = A$ and B. Specifically,

$$q_{\mathbf{k}}(s) = \begin{cases} [\mathbf{T}_A(s)]_{\mathbf{k},0}, & \text{if } s \le f \\ \Sigma_{\mathbf{g}}[\mathbf{T}_B(s-f)]_{\mathbf{k},\mathbf{g}} q_{\mathbf{g}}(f), & \text{if } s > f \end{cases} \tag{23}$$

and similarly

$$\bar{q}_{\mathbf{k}}(s) = \begin{cases} \Sigma_{\mathbf{g}}[\mathbf{T}_A(f-s)]_{\mathbf{k},\mathbf{g}} \bar{q}_{\mathbf{g}}(f), & \text{if } s < f \\ [\mathbf{T}_B(1-s)]_{\mathbf{k},0}, & \text{if } s \ge f \end{cases} \tag{24}$$

Once the partial partition functions are evaluated,

$$\rho_{\mathbf{k}}(s) = \frac{\mathscr{V}}{\mathscr{Q}}\sum_{\mathbf{g}} q_{\mathbf{g}}(s)\bar{q}_{\mathbf{k}-\mathbf{g}}(s) \tag{25}$$

where

$$\mathscr{Q} = \mathscr{V} q_0(1) \tag{26}$$

Now it is a straightforward matter of adjusting $w_{\mathbf{k}}$ and $u_{\mathbf{k}}$ so that

$$\phi_{A;\mathbf{k}} - \phi_{B;\mathbf{k}} = \Phi_{\mathbf{k}} \tag{27}$$

$$\phi_{A;\mathbf{k}} + \phi_{B;\mathbf{k}} = \delta_{\mathbf{k},\mathbf{0}} \tag{28}$$

where

$$\phi_{A;\mathbf{k}} = \int_0^f \rho_{\mathbf{k}}(s)ds \tag{29}$$

$$\phi_{B;\mathbf{k}} = \int_f^1 \rho_{\mathbf{k}}(s)ds \tag{30}$$

Since added constants to the fields have no effect, we are free to set $w_{\mathbf{0}} = u_{\mathbf{0}} = 0$. Once the remaining coefficients for $\mathbf{k} \neq 0$ are

determined, the Landau–Ginzburg free energy is given by

$$\frac{F[\Phi]}{nk_BT} = -\ln\mathscr{Q} - \sum_{\mathbf{k}}\left\{\frac{\chi N}{4}\Phi_{\mathbf{k}}\Phi_{-\mathbf{k}} + w_{\mathbf{k}}\Phi_{-\mathbf{k}} - H_{\mathbf{k}}N\Phi_{-\mathbf{k}}\right\} - \mathscr{E} \tag{31}$$

(Note that we have dropped an irrelevant constant of $\chi N/4$.) The Fourier coefficients for the surface potential are given by

$$H_{\mathbf{k}} = \left\{\Lambda_1 + \Lambda_2 \exp\left(-ik_z D_{\|}\right)\right\}\frac{aN^{1/2}}{D_{\|}} \tag{32}$$

if $k_x = k_y = 0$, and by $H_{\mathbf{k}} = 0$ otherwise.

When expressed in Fourier coefficients, the Maxwell equation (11) becomes a simple set of linear equations,

$$k_z\kappa_{\mathbf{k}} = \sum_{\mathbf{g}}\mathbf{k}\cdot\mathbf{g}\kappa_{\mathbf{k}-\mathbf{g}}v_{\mathbf{g}} \tag{33}$$

After we solve for the coefficients of $v(\mathbf{r})$, the electrostatic energy (8) can be evaluated using

$$\mathscr{E} = \mathscr{E}_D\left[1 + \kappa_\Delta\sum_{\mathbf{k}}k_z\Phi_{\mathbf{k}}v_{-\mathbf{k}}\right] \tag{34}$$

where

$$\mathscr{E}_D = \frac{\varepsilon_0\bar{\kappa}E_0^2\mathscr{V}}{2nk_BT} \tag{35}$$

represents the field energy of a disordered melt and

$$\kappa_\Delta = \frac{\kappa_A - \kappa_B}{2\bar{\kappa}} \tag{36}$$

$$\bar{\kappa} \equiv f\kappa_A + (1-f)\,\kappa_B \tag{37}$$

specify the dielectric contrast and the average dielectric constant, respectively.

Testing the stability of a given morphology requires us to evaluate the change in free energy,

$$\frac{\delta F}{nk_BT} \equiv \frac{F[\Phi+\delta\Phi] - F[\Phi]}{nk_BT} \approx \sum_{\mathbf{k}}\Omega_{\mathbf{k}}\delta\Phi_{-\mathbf{k}} \tag{38}$$

$$+\frac{1}{2}\sum_{\mathbf{k},\mathbf{g}}\left[\mathbf{C}_{RPA}^{-1}\right]_{\mathbf{k},\mathbf{g}}\delta\Phi_{-\mathbf{k}}\delta\Phi_{\mathbf{g}} \tag{39}$$

produced by a small variation, $\delta\Phi(\mathbf{r})$, in the composition profile.[15] The only complicated step is determining the corresponding variation in the fields, $\delta w(\mathbf{r})$ and $\delta u(\mathbf{r})$, which is done using the identities,[18]

$$\frac{\partial\ln\mathscr{Q}}{\partial w_{-\mathbf{k}}} = -\left(\phi_{A;\mathbf{k}} - \phi_{B;\mathbf{k}}\right) \tag{40}$$

$$\frac{\partial\ln\mathscr{Q}}{\partial u_{-\mathbf{k}}} = -\left(\phi_{A;\mathbf{k}} + \phi_{B;\mathbf{k}}\right) \tag{41}$$

The variation in $\ln\mathscr{Q}$ is first expanded in a Taylor series as

$$-\delta\ln\mathscr{Q} \approx \sum_{\mathbf{k}}\Phi_{\mathbf{k}}\delta w_{-\mathbf{k}} - \frac{1}{2}\sum_{\mathbf{k},\mathbf{g}}\left[\mathbf{C}_{\mathbf{k},\mathbf{g}}\delta w_{-\mathbf{k}}\delta w_{\mathbf{g}} + 2\mathbf{\Delta}_{\mathbf{k},\mathbf{g}}\delta w_{-\mathbf{k}}\delta u_{\mathbf{g}} + \Sigma_{\mathbf{k},\mathbf{g}}\delta u_{-\mathbf{k}}\delta u_{\mathbf{g}}\right] \tag{42}$$

where the matrices for the second-order terms are evaluated by numerical differentiation of eqn (40) and (41). (Note that $\mathbf{C}$ and $\mathbf{\Sigma}$ are both Hermitian, but $\mathbf{\Delta}$ is not.) In order to maintain the incompressibility, the derivative of $\delta\ln\mathscr{Q}$ with respect to $\delta u_{-\mathbf{k}}$ must be zero, which requires

$$\delta u_{\mathbf{k}} = -\sum_{\mathbf{g}}\left[\mathbf{\Sigma}^{-1}\mathbf{\Delta}^{\dagger}\right]_{\mathbf{k},\mathbf{g}}\delta w_{\mathbf{g}} \tag{43}$$

Next the derivative with respect to $\delta w_{-\mathbf{k}}$ must equal $-(\Phi_{\mathbf{k}} + \delta\Phi_{\mathbf{k}})$, which implies

$$\delta w_{\mathbf{k}} = -\sum_{\mathbf{g}}\left[\tilde{\mathbf{C}}^{-1}\right]_{\mathbf{k},\mathbf{g}}\delta\Phi_{\mathbf{g}} \tag{44}$$

where

$$\tilde{\mathbf{C}} \equiv \mathbf{C} - \mathbf{\Delta}\mathbf{\Sigma}^{-1}\mathbf{\Delta}^{\dagger} \tag{45}$$

Now that the change in the fields is known, it is a simple matter of substituting the results into eqn (38) using the free energy expression in eqn (31). The first-order coefficients in eqn (39) come out as

$$\Omega_{\mathbf{k}} = -w_{\mathbf{k}} - \frac{\chi N}{2}\Phi_{\mathbf{k}} - H_{\mathbf{k}}N - \frac{\partial\mathscr{E}}{\partial\Phi_{-\mathbf{k}}} \tag{46}$$

where the derivatives of $\mathscr{E}$ are given by

$$\frac{\partial\mathscr{E}}{\partial\Phi_{-\mathbf{k}}} = -\mathscr{E}_D\kappa_\Delta\left[2k_zv_{\mathbf{k}} + \sum_{\mathbf{g}}\mathbf{g}\cdot(\mathbf{g}+\mathbf{k})v_{\mathbf{g}+\mathbf{k}}v_{-\mathbf{g}}\right] \tag{47}$$

The second-order coefficients in the expansion (39) take the form,

$$\left[\mathbf{C}_{RPA}^{-1}\right]_{\mathbf{k},\mathbf{g}} = \left[\tilde{\mathbf{C}}^{-1}\right]_{\mathbf{k},\mathbf{g}} - \frac{\chi N}{2}\delta_{\mathbf{k},\mathbf{g}} - \frac{\partial^2\mathscr{E}}{\partial\Phi_{-\mathbf{k}}\partial\Phi_{\mathbf{g}}} \tag{48}$$

This time, there is no simple expression for the second derivatives of $\mathscr{E}$, and so we obtain them by numerical differentiation of eqn (47).

A stable or metastable block copolymer morphology, $\Phi(\mathbf{r})$, must represent a minimum in the free energy surface, $F[\Phi]$. The first requirement for a minimum is that the gradient of the free energy surface be zero, which amounts to $\Omega_{\mathbf{k}} = 0$. This corresponds to the usual self-consistent field equation that gives SCFT its name. The second requirement, which is generally not tested, is that the eigenvalues, λ_α, of $\mathbf{C}_{RPA}^{-1}$ are positive for all wavelengths, $D_\perp$. If an eigenvalue becomes negative, the free energy surface develops a saddle shape, allowing the system to lower its free energy by evolving $\Phi(\mathbf{r})$ in the direction of the associated eigenvector, $\delta\Phi_\alpha(\mathbf{r})$.

Our study is in principle very simple; we first locate the self-consistent solution for parallel lamellae by adjusting the field coefficients, $w_{\mathbf{k}}$ and $u_{\mathbf{k}}$, so that $\Omega_{\mathbf{k}} = 0$ and $\boldsymbol{\phi}_{\mathrm{A};\mathbf{k}} + \boldsymbol{\phi}_{\mathrm{B};\mathbf{k}} = 0$, for all $\mathbf{k} \neq 0$. Because the lamellae are uniform in the $\hat{\mathbf{e}}_x$ direction,

we can ignore wavevectors with $k_x \neq 0$. Still there are an infinite number of wavevectors, and so we truncate the ones with $|k_z|$ greater than some cut-off. We are careful to ensure that the cut-off is sufficiently large that the resulting numerical inaccuracy is irrelevant on the scale of our plots. Once the self-consistent solution is known, we then calculate $\mathbf{C}_{RPA}^{-1}$ and its dominant (*i.e.*, smallest) eigenvalue, λ_1, as a function of lateral periodicity, $D_\perp$. For this step, we use the same range of k_z, but now we allow $k_x = 0$ and $\pm 2\pi/D_\perp$.

3. Results

The case of monolayer ($v = 1$) films was investigated thoroughly in our previous study,[16] and so we now turn our attention to multilayer ($v > 1$) films. To facilitate comparison with the earlier calculations, we select similar parameters where, for example, the diblock copolymers are both compositionally symmetric ($f = 0.5$) and conformationally symmetric ($a_A = a_B \equiv a$). As before, we assume the lamellae are prepared with their natural bulk periodicity, D_b, such that $D_\parallel = vD_b$. Without loss of generality, the film morphology is chosen with B-rich lamellae next to the plates, although we do not explicitly include a surface affinity ($\Lambda_1 = \Lambda_2 = 0$) because it has no significant effect on the instability modes. Although our sample calculations are generally performed for the specific intermediate segregation of $\chi N = 15$ and dielectric contrast of $|\kappa_\Delta| = 0.4$, we will investigate the effects of χN and κ_Δ on our main predictions.

To begin, Fig. 2 plots the dominant eigenvalue, λ_1, of $\mathbf{C}_{RPA}^{-1}$ as a function of lateral periodicity. Results are shown for the finite film thicknesses of $v = 1$, 2, and 4, as well as for the asymptotic limit (*i.e.*, $v \to \infty$) corresponding to a bulk melt. (Note that the bulk condition is simulated by switching from reflecting to periodic boundary conditions in the $\hat{\mathbf{e}}_z$ direction.) In this specific example, we have fixed the electric field strength at $\mathscr{E}_D = 2$ and the dielectric contrast at $|\kappa_\Delta| = 0.4$. As demonstrated in our previous paper, the λ_1 for monolayer films is significantly reduced for positive κ_Δ, where the central A-rich domain has the higher dielectric constant. In contrast, the λ_1 for multilayer films is absolutely unaffected by the sign

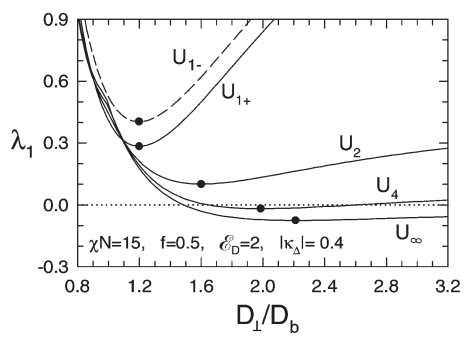

Fig. 2 Dominant eigenvalue of $\mathbf{C}_{RPA}^{-1}$ corresponding to the undulatory (U_v) mode in a v-layer stack of parallel lamellae plotted as a function of lateral periodicity, $D_\perp$, relative to the bulk lamellar period, D_b. U_{1+} and U_{1-} denote the undulatory modes for a monolayer with $\kappa_\Delta = 0.4$ and -0.4, respectively; all the other modes are unaffected by the sign of κ_Δ. The minima indicated by the solid dots are referred to as λ_1^* and $D_\perp^*$.

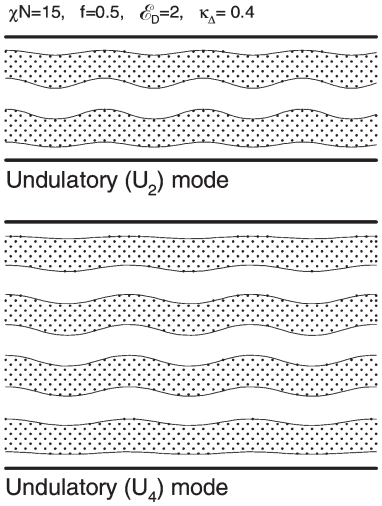

Fig. 3 Undulatory (U_v) modes for $v = 2$ and 4 at the preferred periodicities, $D_\parallel^*$, denoted by solid dots in Fig. 2. These modes are calculated for $\kappa_\Delta = 0.4$, where the shaded A-rich domains possess the higher dielectric constant; the modes for $\kappa_\Delta = -0.4$ are slightly different, although the difference would be difficult to detect on this scale.

of κ_Δ, assuming that the diblock copolymers are perfectly symmetric (*i.e.*, $f = 0.5$ and $a_A = a_B$).

Fig. 3 demonstrates that the dominant eigenvalue, λ_1, does indeed correspond to an undulatory mode. The diagrams are obtained by adding 10% of the corresponding normalized eigenvector, $\delta\Phi_1(\mathbf{r})$, to the lamellar profile, $\Phi(\mathbf{r})$. The interface between the A- and B-rich domains is then defined by $\Phi(\mathbf{r}) + 0.1 \times \delta\Phi_1(\mathbf{r}) = 0$. In each case, we have plotted the mode at the preferred periodicity, $D_\perp^*$, denoted by the solid dots in Fig. 2. Although the sign of κ_Δ does not affect the eigenvalue λ_1, it does alter the detailed shape of the mode by reversing the sign of some but not all the Fourier coefficients of the eigenvector $\delta\Phi_1(\mathbf{r})$. Nevertheless, the difference in shape is nearly indistinguishable on the scale of Fig. 3, which is why we only show the modes for positive κ_Δ.

The curves for the dominant eigenvalue all display a minimum, λ_1^*, at a preferred periodicity, $D_\perp^*$, denoted by solid dots in Fig. 2. The effect of the electric field on λ_1^* and $D_\perp^*$ is demonstrated in Fig. 4. Regardless of the film thickness v, the electric field causes a significant reduction in λ_1^*, which is accompanied by a contraction in $D_\perp^*$. Eventually a critical field strength, $\mathscr{E}_D^*$, is reached, where $\lambda_1^* = 0$. At this point, the electric field has become so strong that not only do the parallel lamellae no longer represent the equilibrium state, they are not even metastable. The undulation mode will grow in spontaneously causing the film to evolve towards another lower-energy morphology, although not necessarily the equilibrium morphology of perpendicular lamellae.

The solid dots in Fig. 4 illustrate the procedure for calculating the critical field strengths, $\mathscr{E}_D^*$, and the corresponding wavelengths, $D_\perp^*$, at which lamellar stacks of various thicknesses go unstable. The rest of this section will focus on these two quantities as they represent the threshold required to initiate the reorientation of the lamellae. Fig. 5 shows the effect of segregation, χN, on both quantities. In all cases, the critical

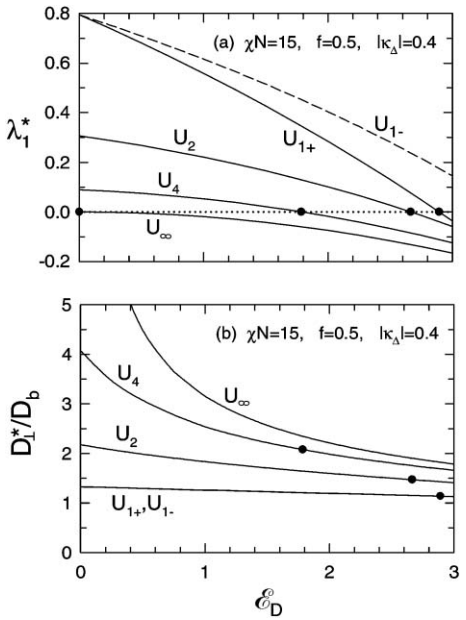

Fig. 4 (a) Dominant eigenvalue of $\mathbf{C}_{RPA}^{-1}$ evaluated at the preferred lateral periodicity and plotted as a function of the field strength, $\mathscr{E}_D$. The solid dots denote the critical field strength, $\mathscr{E}_D^*$. (b) Preferred lateral periodicity, $D_\perp^*$, relative to the bulk lamellar period, D_b. The solid dots denote the periodicity at the critical field strength.

field increases monotonically from zero starting at χN = 10.495, the bulk order-disorder transition (ODT).[17] Note that in the weak-segregation regime ($\chi N \sim 12$), there are peristaltic modes that compete with the undulation modes. We will mention more about the peristaltic modes in the next section, but their competition with the undulation modes is not

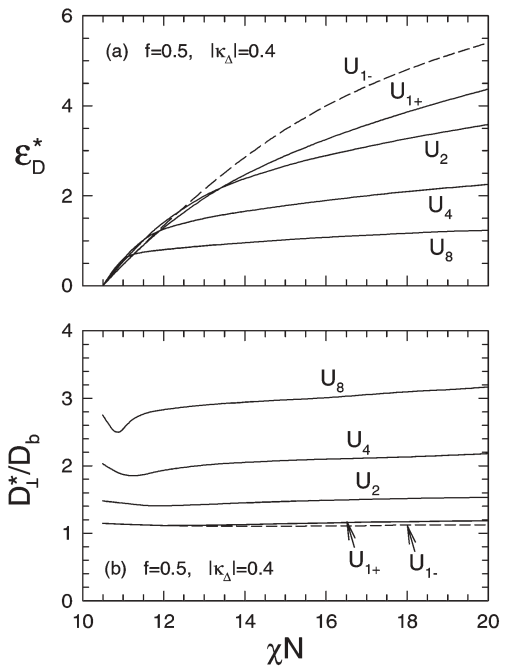

Fig. 5 (a) Critical field strength, $\mathscr{E}_D^*$, for the undulatory (U_v) modes plotted as a function of the block copolymer segregation, χN. (b) Lateral periodicity, $D_\perp^*$, relative to the bulk lamellar period, D_b.

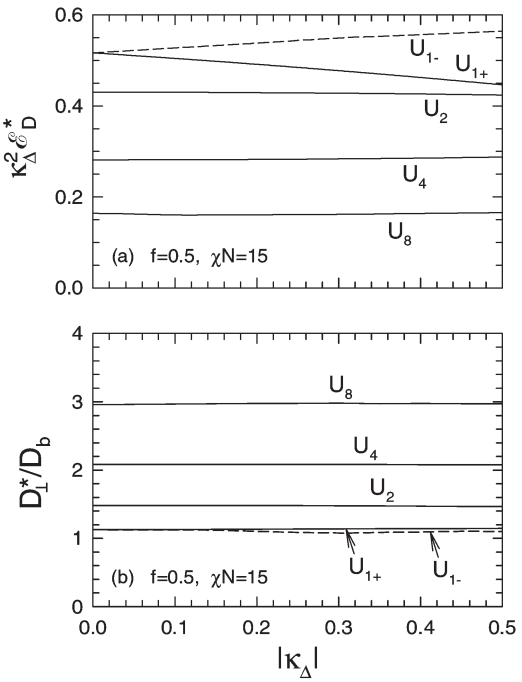

Fig. 6 (a) Critical field strength, $\mathscr{E}_D^*$, for the undulatory (U_v) modes plotted as a function of the dielectric contrast, $|\kappa_\Delta|$. (b) Lateral periodicity, $D_\perp^*$, relative to the bulk lamellar period, D_b.

investigated here since, in any case, weak-segregation behaviour is significantly modified by thermal (Brazovskii) fluctuations,[18,19] which are neglected by mean-field theories.

So far, our calculations have been limited to dielectric contrasts of $|\kappa_\Delta| = 0.4$, which is the approximate value for the PS-PMMA diblock copolymers examined by Xu *et al.*[13,14] Fig. 6 now shows the effect on $\mathscr{E}_D^*$ and $D_\perp^*$ of changing $|\kappa_\Delta|$ while holding the level of segregation fixed at $\chi N = 15$. Notice that we have scaled the vertical axis in Fig. 6a with respect to κ_Δ^2. This is motivated by a common approximation for the electrostatic energy,[10] whereby $\mathscr{E} \propto \kappa_\Delta^2 \mathscr{E}_D$. Consistent with this prediction, the curves in Fig. 6b are virtually constant, apart from the monolayer mode (v = 1), which incidentally is the only one affected by the sign of κ_Δ.

4. Discussion

In our previous study on monolayer films,[16] we identified two competing instabilities, an undulatory mode, like those examined in our present study, plus a peristaltic mode. In contrast to the undulatory mode where the central lamellae undulates with a relatively uniform thickness, the peristaltic mode involves modulations in the lamellar thickness (*i.e.*, a periodic sequence of bulges and constrictions). The multilayer films also display peristaltic instabilities where the various lamellae develop modulations in their thickness, but it becomes a set of modes due to the different possible phase relations between adjacent layers. In any case, these peristaltic modes are nearly degenerate in energy with that of the monolayer, because there is no significant energetic advantage to be had by correlating the modulations of one lamella with those of its neighbours. This is in stark contrast to the undulatory modes.

By undulating in unison (*i.e.*, no phase difference between layers), the individual lamellae maintain a reasonably uniform thickness thus minimizing their elastic distortion. The only exceptions are those lamellae next to the plates, but of course their presence becomes less and less important the more layers ν there are in the film. This is the root explanation of why the undulation mode becomes increasingly unstable for thicker films.

The critical field strength, $\mathscr{E}_{\mathrm{D}}^{*}$, represents the point beyond which even perfectly formed parallel lamellae become unstable and necessarily transform to some lower-energy morphology. If defects are present, then the parallel lamellae will succumb to the influences of the electric field at even lower values of $\mathscr{E}_{\mathrm{D}}$.[20] In general, the surface affinity does not significantly affect $\mathscr{E}_{\mathrm{D}}^{*}$, simply because small amplitude undulations do not alter the surface coverage as evident from Fig. 3. This is why we have not included results for nonzero Λ_1 and Λ_2. Of course, the surface potential will eventually influence the undulations once their amplitude becomes large enough to affect the segment concentration at the plates, but the evolution of the unstable morphologies is beyond the scope of our present study.

The earlier phenomenological calculation by Onuki and Fukuda[12] is less predictive and less accurate than our approach. For example, their predictions are in terms of the effective elastic moduli of the lamellae[15] rather than the molecular parameters. Furthermore, they make a number of approximations in their treatment of the electric field including the assumption that the segment profile, $\Phi(\mathbf{r})$, varies sinusoidally. Nevertheless, the advantage of their approach is that it provides the simple analytical expression,

$$\lambda_1 \propto \frac{1}{D_{\|}^2} + \frac{D_b^2}{D_{\perp}^2}\left(\frac{1}{D_{\perp}^2} - \alpha\kappa_{\Delta}^2\mathscr{E}_D\right) \tag{49}$$

where α is a constant that depends on the phenomenological parameters of the model. From this, it follows that the preferred periodicity of an undulation is

$$D_{\perp}^{*} = \sqrt{\frac{2}{\alpha\kappa_{\Delta}^2\mathscr{E}_D}} \tag{50}$$

for which the eigenvalue becomes

$$\lambda_1^{*} \propto \frac{1}{D_{\|}^2} - \frac{D_b^2}{4}\left(\alpha\kappa_{\Delta}^2\mathscr{E}_D\right)^2 \tag{51}$$

This predicts a critical field of

$$\kappa_{\Delta}^2\mathscr{E}_D^{*} = \frac{2}{\alpha D_{\|} D_b} = \frac{2}{\alpha\nu D_b^2} \tag{52}$$

for which the preferred periodicity reduces to

$$D_{\perp}^{*} = \sqrt{D_{\|} D_b} = \sqrt{\nu} D_b \tag{53}$$

These expressions do capture the general qualitative tends exhibited by our SCFT predictions, although there are some significant differences. For instance, eqn (49) implies that a change in the film thickness, $D_{\|} = \nu D_{\mathrm{b}}$, just adds a constant to λ_1, which in turn implies that $D_{\perp}^{*}$ remains fixed. Both of these predictions are clearly wrong according to Fig. 2 and 4b, respectively. The analytical eqn (52) also suggests that the critical field, $\mathscr{E}_{\mathrm{D}}^{*}$, is proportional to ν^{-1}, which is a significantly stronger dependence than predicted in Fig. 5a and 6a. On the other hand, the prediction by eqn (52) that $\mathscr{E}_{\mathrm{D}}^{*} \propto \kappa_{\Delta}^{-2}$ is remarkably consistent with Fig. 6a, provided that $\nu > 1$. Most impressive though is the explicit prediction in eqn (53) not involving the phenomenological constant α, which agrees rather well with the preferred periodicities plotted in Fig. 5b and 6b.

In addition to their stability analysis, Onuki and Fukuda[12,21] have also examined the kinetics that occur once the critical field strength is exceeded. To do this, they assume that the order parameter, $\Phi(\mathbf{r})$, varies according to simple Langevan dynamics.[21] Likewise, this can also be done within the framework of SCFT, and in fact Zvelindovsky and coworkers[20,22,23] have already performed such calculations. However, their SCFT treatment is done in real space using a coarse mesh combined with an approximate treatment of the Maxwell equation. Therefore, it would be nice to adapt the Langevan dynamics to our Fourier approach; the only problem would be the computational cost of examining sufficient system sizes to allow the competition between modes with different lateral periodicities. This problem could be remedied with the semi-spectral technique of Rasmussen and Kalosakas,[24] as it would permit the electric potential to be solved exactly using the spectral representation in eqn (33) while avoiding the need to evaluate the transfer matrices, $\mathbf{T}_{\gamma}(s)$, which becomes a formidable task due to the vast number of wavevectors required for large system sizes.

An advantage of our microscopic SCFT approach over the phenomenological one is the ability to make direct comparisons with experiment. We now demonstrate this by relating our predictions to the measurements of Xu *et al.*.[13,14] They examined films with thicknesses of ν = 4, 10, 23, and 100, consisting of symmetric PS-PMMA diblocks at a segregation of $\chi N \approx 26$. Unfortunately, they applied their electric field, E_0 = 40 V $\mu\mathrm{m}^{-1}$, before the films had a chance to form well-ordered parallel lamellae. Given the abundance of defects, the growth of perpendicular lamellae does not necessarily imply that $E_0 > E_0^{*}$. On the other hand, the ν = 4 and 10 films transformed from relatively disordered states into well-ordered parallel lamellae, which implies that the final states are equilibrium (*i.e.*, global free-energy minimum) as opposed to merely metastable (*i.e.*, local free-energy minimum). This not only implies that $E_0 < E_0^{*}$, but that E_0 is significantly smaller than E_0^{*}. Thus, this is an inequality that we can test. Based on mild extrapolations of our results in Fig. 5a, the critical field for a ν = 10 film should occur at $\kappa_{\Delta}^2\mathscr{E}_{\mathrm{D}}^{*} \approx 0.2$. To convert this to an actual electric field, we set κ_{Δ} = 0.42, $\bar{\kappa}$ = 4.3, and $\mathscr{V}/n$ = 114 nm^3 using values quoted in ref. 13. The resulting critical field, E_0 = 57 V $\mu\mathrm{m}^{-1}$, is indeed significantly larger than the applied field, E_0 = 40 V $\mu\mathrm{m}^{-1}$, but not by much.

Previous calculations by Tsori *et al.*,[25] using weak-segregation theory coupled with an approximate treatment of the electrostatic energy, predict that the dielectric mechanism is too feeble to account for the experimental results on PS-PMMA diblock copolymers. This motivated Tsori and

co-workers to incorporate an added mechanism, involving Li^+ ions dissociated from the PMMA blocks, that is estimated to be orders-of-magnitude stronger than the bare dielectric mechanism. However, our more refined SCFT-based calculations now show that the dielectric mechanism alone is sufficient to explain the behaviour of the $v = 10$ film discussed above. In fact, the free-ion mechanism, as suggested in ref. 25, would undoubtedly lower $E_0^* = 57$ V μm^{-1} to something much less than the applied $E_0 = 40$ V μm^{-1}, thus creating a serious disagreement with experiment. We have some concerns regarding the assumptions behind the proposed mechanism for ions; in particular, we belief that any dissociated Li^+ ions would not remain in the PMMA domains, but would be swept to the negative electrode given that the applied field is close to that of dielectric breakdown. In any case, the obvious way of discriminating between the two mechanisms is to apply high-frequency ac electric fields; the dielectric mechanism should only exhibit a mild dependence on frequency while the free-ion mechanism would effectively turn off.[26] Recent experiments[27] of this type indicate an absence of free ions in PMMA samples, although they do provide evidence for free ions when the PMMA is loaded with extra lithium. Perhaps the strongest evidence though is that provided by earlier experiments[28] on thin homopolymer films, which not only exhibit similar results for ac and dc fields but also agree with a parameter-free model based on the dielectric mechanism.

Presumably, Xu *et al.*[13] applied the electric field in their experiment while the films were still in a relatively disordered state so as to maximise the likelihood of forming perpendicular lamellae. However, in the interest of providing a more conclusive quantitative test of the theory, it would be desirable to examine the effect of electric fields on well-ordered parallel lamellae with various film thicknesses, $D_{\|} = vD_b$. In principle, this would only require that Xu and co-workers delay the application of the electric field until the film had time to order, although there are a couple of other modifications that could help. For instance, a small shearing of the plates might remove any residual defects from the parallel lamellae. Preparing samples in clean-room conditions should also reduce the problem of dielectric breakdown, allowing access to higher values of $\mathscr{E}_D$.[29]

Note that there have also been related experiments by Böker *et al.*,[22,30] but on thick films with added solvent. In this case, reorientation of the lamellae is observed using relatively small electric fields of 1 V μm^{-1}. The larger thickness of their films is one reason for the reduced field, but the more significant factors are probably due to the solvent. In addition to diluting the polymer domains and speeding up the dynamics, we anticipate a number of other interesting effects. For example, the solvent should relieve the packing frustration that penalizes variations in domain thickness.[31] Also the mobility of the solvent molecules will allow the system new ways of adjusting $\kappa(\mathbf{r})$. In light of the possibilities, there is clear motivation for extending our present study to include solvent. Indeed, this is a straightforward extension of SCFT,[32] and the fact that it can be done explicitly means that the predictions should be most informative. The same cannot be said of the Onuki–Fukuda approach, where an added solvent would simply modify the phenomenological parameters of the model in some unspecified way. This simple adjustment of the model parameters will not be enough to account for subtle issues such as packing frustration and the nontrivial redistribution of solvent.

5. Conclusions

We have examined the undulation mode in films of parallel lamellae and calculated the critical electric field, E_0^*, beyond which the mode becomes unstable. Analogous calculations have been performed by Onuki and Fukuda[12] using a phenomenological model for the effective elasticity of the lamellae coupled with an approximate treatment of the electric field. In contrast, our SCFT-based approach performs exact mean-field calculations on a microscopic model, specifically the standard Gaussian chain model,[17] in combination with exact solutions of the Maxwell equation for the electric field. While our results remain qualitatively similar to those of Onuki and Fukuda, there are some significant differences in the details.

Not only is our treatment more accurate, the fact that it is based on a microscopic model facilitates direct quantitative comparison with experiment. At the moment, the most relevant experiments are those of Xu *et al.*[13,14] examining symmetric PS-PMMA diblock copolymer films of various thicknesses annealed under an electric field of $E_0 = 40$ V μm^{-1}. They have shown that films of $v \leqslant 10$ parallel lamellae are stable even with the presence of numerous defects, which is consistent with our estimated value of $E_0^* = 57$ V μm^{-1} for $v = 10$. This agreement removes the need to invoke additional mechanisms, such as the one involving free ions.[25] Still this does not rule out the possibility that this and other mechanisms are involved in the reorientation of block copolymer domains by electric fields. To confirm the actual underlying physics will require further experiments, preferably ones that make quantitative comparisons with theory on films of well-defined morphology such as defect-free lamellae.

References

1 F. S. Bates and G. H. Fredrickson, *Phys. Today*, 1999, **52**, 32.
2 I. W. Hamley, *Nanotechnology*, 2003, **14**, R39.
3 (*a*) S. A. Jenekha and X. L. Chen, *Science*, 1999, **283**, 372; (*b*) A. S. Zalusky, R. Olayo-Valles, J. H. Wolf and M. A. Hillmyer, *J. Am. Chem. Soc.*, 2002, **124**, 12761.
4 D. Zhao, J. Feng, Q. Huo, N. Melosh, G. H. Fredrickson, B. F. Chmelka and G. D. Stucky, *Science*, 1998, **279**, 548.
5 (*a*) M. Templin, A. Franck, A. DuChesne, H. Leist, Y. M. Zhang, R. Ulrich, V. Schadler and U. Wiesner, *Science*, 1997, **278**, 1795; (*b*) W. A. Lopes and H. M. Jaeger, *Nature*, 2001, **414**, 735.
6 M. Park, C. Harrison, P. M. Chaikin, R. A. Register, D. H. Adamson and N. Yao, *Science*, 1997, **276**, 1401.
7 J. T. Chen, E. L. Thomas, C. G. Zimba and J. F. Rabolt, *Macromolecules*, 1995, **28**, 5811.
8 T. Thurn-Albrecht, J. Schotter, C. A. Kastle, N. Emley, T. Shibauchi, L. Krusin-Elbaum, K. Guarini, C. T. Black, M. T. Tuominen and T. P. Russell, *Science*, 2000, **290**, 2126.
9 (*a*) P. Mansky, Y. Lui, E. Haung, T. P. Russell and C. Hawker, *Science*, 1997, **275**, 1458; (*b*) J. Genzer and E. J. Kramer, *Phys. Rev. Lett.*, 1997, **78**, 4946.
10 (*a*) K. Amundson, E. Helfand, X. N. Quan and S. D. Smith, *Macromolecules*, 1993, **26**, 2698; (*b*) K. Amundson, E. Helfand, X. N. Quan, S. D. Hudson and S. D. Smith, *Macromolecules*, 1994, **27**, 6559.

11 T. L. Morkved, M. Lu, A. M. Urbas, E. E. Ehrichs, H. M. Jaeger, P. Mansky and T. P. Russell, *Science*, 1996, **273**, 931.
12 A. Onuki and J. Fukuda, *Macromolecules*, 1995, **28**, 8788.
13 T. Xu, C. J. Hawker and T. P. Russell, *Macromolecules*, 2003, **36**, 6178.
14 T. Xu, Y. Zhu, S. P. Gido and T. P. Russell, *Macromolecules*, 2004, **37**, 2625.
15 C. Yeung, A.-C. Shi, J. Noolandi and R. D. Desai, *Macromol. Theory Sim.*, 1996, **5**, 291.
16 M. W. Matsen, *Phys. Rev. Lett.*, 2005, **95**, 258302.
17 M. W. Matsen, *J. Phys.: Condens. Matter*, 2001, **14**, R21.
18 M. W. Matsen, in *Soft Matter*, ed. G. Gompper and M. Schick, Wiley-VCH, Weinheim, 2006, vol. 1, ch. 2.
19 G. H. Fredrickson and E. Helfand, *J. Chem. Phys.*, 1987, **87**, 697.
20 K. Schmidt, A. Böker, H. Zettl, F. Schubert, H. Hänsel, F. Fischer, T. M. Weiss, V. Abetz, A. V. Zvelindovsky, G. J. A. Sevink and G. Krausch, *Langmuir*, 2005, **21**, 11974.
21 J. Fukuda and A. Onuki, *J. Phys. II*, 1995, **5**, 1107.
22 A. Böker, H. Elbs, H. Hänsel, A. Knoll, S. Ludwigs, H. Zettl, A. V. Zvelindovsky, G. J. A. Sevink, V. Urban, V. Abetz, A. H. E. Müller and G. Krausch, *Macromolecules*, 2003, **36**, 8078.
23 A. V. Kyrylyuk, A. V. Zhelindowsky, G. J. A. Sevink and J. G. E. M. Fraaije, *Macromolecules*, 2002, **35**, 1473.
24 K. O. Rasmussen and G. Kalosakas, *J. Polym. Sci., Part B*, 2002, **40**, 1777.
25 Y. Tsori, F. Tournilhac, D. Andelman and L. Leibler, *Phys. Rev. Lett.*, 2003, **90**, 145504.
26 Y. Tsori, F. Tournilhac and L. Leibler, *Macromolecules*, 2003, **36**, 5873.
27 J.-Y. Wang, T. Xu, J. M. Leiston-Belanger, S. Gupta and T. P. Russell, *Phys. Rev. Lett.*, 2006, **96**, 128301.
28 E. Schäffer, T. Thurn-Albrecht, T. P. Russell and U. Steiner, *Europhys. Lett.*, 2001, **53**, 518.
29 U. Steiner is able to apply electric fields of 100–150 V μm^{-1}, and believes there is scope for a further increase; private communication.
30 A. Böker, H. Elbs, H. Hänsel, A. Knoll, S. Ludwigs, H. Zettl, V. Urban, V. Abetz, A. H. E. Müller and G. Krausch, *Phys. Rev. Lett.*, 2002, **89**, 135502.
31 M. W. Matsen and F. S. Bates, *Macromolecules*, 1996, **29**, 7641.
32 J. R. Naughton and M. W. Matsen, *Macromolecules*, 2002, **35**, 5688.

